








# GROWTH on S190426c II: GROWTH-India Telescope search for an optical counterpart with a custom image reduction and candidate vetting pipeline

Harsh Kumar <sup>1,★†</sup>, Varun Bhalariao,<sup>1</sup> G. C. Anupama <sup>2</sup>, Sudhanshu Barway <sup>2</sup>, Michael W. Coughlin <sup>3</sup>, Kishalay De,<sup>4,5</sup> Kunal Deshmukh,<sup>6</sup> Anirban Dutta,<sup>2</sup> Daniel A Goldstein,<sup>4</sup> Adeem Jassani,<sup>1</sup> Simran Joharle,<sup>7</sup> Viraj Karambelker,<sup>4</sup> Maitreya Khandagale,<sup>1</sup> Brajesh Kumar <sup>2,8</sup>, Divita Saraogi,<sup>1</sup> Yashvi Sharma,<sup>4</sup> Vedant Shenoy,<sup>1</sup> Leo singer <sup>9,10</sup>, Avinash Singh <sup>2,11</sup> and Gaurav Waratkar<sup>1</sup>

<sup>1</sup>Physics Department, Indian Institute of Technology Bombay, Powai 400 076, India

<sup>2</sup>Indian Institute of Astrophysics, 2nd Block 100 Feet Rd, Koramangala Bangalore 560 034, India

<sup>3</sup>School of Physics and Astronomy, University of Minnesota, Minneapolis, Minnesota 55455, USA

<sup>4</sup>Division of Physics, Mathematics, and Astronomy, California Institute of Technology, Pasadena, CA 91125, USA

<sup>5</sup>MIT-Kavli Institute for Astrophysics and Space Research, 77 Massachusetts Ave., Cambridge, MA 02139, USA

<sup>6</sup>Department of Physics and Astronomy, Texas Tech University, PO Box 41051, Lubbock, TX 79409, USA

<sup>7</sup>Heidelberg University, Grabengasse 1, D-691 17 Heidelberg, Germany

<sup>8</sup>Aryabhata Research Institute of Observational Sciences, Manora Peak, Nainital 263 001, India

<sup>9</sup>Astrophysics Science Division, NASA Goddard Space Flight Center, Greenbelt, MD 20771, USA

<sup>10</sup>Joint Space-Science Institute, University of Maryland, College Park, MD 20742, USA

<sup>11</sup>Hiroshima Astrophysical Science Center, Hiroshima University, Higashi-Hiroshima, Hiroshima 739-8526, Japan

Accepted 2022 August 31. Received 2022 August 31; in original form 2022 July 26

## ABSTRACT

S190426c/GW190426.152155 was the first probable neutron star–black hole merger candidate detected by the LIGO-Virgo Collaboration. We undertook a tiled search for optical counterparts of this event using the 0.7-m GROWTH-India Telescope. Over a period of two weeks, we obtained multiple observations over a 22.1 deg<sup>2</sup> area, with a 17.5 per cent probability of containing the source location. Initial efforts included obtaining photometry of sources reported by various groups, and a visual search for sources in all galaxies contained in the region. Subsequently, we have developed an image subtraction and candidate vetting pipeline with  $\sim 94$  per cent efficiency for transient detection. Processing the data with this pipeline, we find several transients, but none that are compatible with kilonova models. We present the details of our observations, the working of our pipeline, results from the search, and our interpretations of the non-detections that will work as a pathfinder during the O4 run of LVK.

**Key words:** methods: data analysis – techniques: image processing – black hole - neutron star mergers – neutron star mergers.

## 1 INTRODUCTION

Coalescing compact object binaries are the primary sources of gravitational waves (GW) for the current ground-based GW detector networks (LIGO Scientific Collaboration et al. 2015; Abbott et al. 2016; Losurdo 2017; Abbott et al. 2017a; KAGRA Collaboration et al. 2021). Such events have been a subject of great interest in astronomy over the last decade, especially since the first-ever detection of GW by the LIGO-Virgo Collaboration (LVC) on 2015 September 14, from a binary black hole merger event (Abbott et al. 2016). Such merger events are accompanied by electromagnetic emission when at least one of the merger candidates is a suitable mass neutron star (Cutler & Thorne 2002; Metzger et al. 2010; Tanaka et al. 2013). The discovery of the first BNS merger event GW170817 has laid out a robust foundation for these claims (Coulter

et al. 2017; Evans et al. 2017; Kasliwal et al. 2017; Abbott et al. 2017c). LIGO and Virgo detected this event during Observation run 2 (O2; Abbott et al. 2017b). This event was accompanied by electromagnetic emission spanning the entire spectrum, starting from gamma-ray emission in the form of a short Gamma-Ray Burst GRB 170817A (Goldstein et al. 2017; Abbott et al. 2017d; Lamb & Kobayashi 2018) just  $\sim 2$  s after the GW, followed by high and low-energy X-ray afterglow emission (D’Avanzo et al. 2018). The UV, optical, and IR counterparts in the form of a kilonova (KN; Valenti et al. 2017) were detected hours after the GW signal. At later times, emission was detected at much longer wavelengths in non-thermal radio bands (Hallinan et al. 2017; Kasliwal et al. 2017; Nakar et al. 2018; Ghirlanda et al. 2019). This event has proven to be a role model for research in this field over the last few years. To date, this is the only GW event with a confirmed EM counterpart. The near simultaneous detection of GW and short-GRB signals from the GW170817 event ushered in new era of multimessenger astronomy. The optical and IR observations of the counterpart ‘AT2017gfo’

\* E-mail: [harshkosli13@gmail.com](mailto:harshkosli13@gmail.com)

† LSSTC DSFP Fellow-2018.

**Table 1.** Initial and revised classification of S190426c candidate event by LVC. (Ligo Scientific Collaboration & VIRGO Collaboration 2019a,c). Note that the event is contained in the final catalog..

Type	Classification probability	
	Initial	Revised
BNS	49 per cent	24 per cent
NSBH	13 per cent	6 per cent
MassGap	24 per cent	12 per cent
Terrestrial	14 per cent	58 per cent
BBH	0 per cent	< 1 per cent

helped in getting an independent measurement of the expansion rate of the universe (Hotokezaka et al. 2019; Coughlin et al. 2020), constraining the equation of state (Radice et al. 2018; Dietrich et al. 2020), radius and mass estimation of the neutron stars (Margalit & Metzger 2017; Rezzolla, Most & Weih 2018; Coughlin et al. 2019b), and established that such merger sites are the factories of the heavy r-process elements in the universe (Drout et al. 2017; Lippuner et al. 2017; Pian et al. 2017). In order to further understand the physics of such an event, more GW170817-like detections are required in EM bands.

During the first half of the third observing run (O3a), the GW networks detected a gravitational wave event named ‘S190426c’/GW190426\_152155 (S190426c hereafter; The LIGO Scientific Collaboration et al. 2021) with a non-zero probability of the event being a merger of a neutron star and a black hole (NSBH). In search of the optical counterpart of the event, we followed up this event with the GROWTH-India Telescope (GIT; Kumar et al. 2022), acquiring data for ten nights. We developed our image subtraction and candidate vetting pipeline for the analysis of this data. In this article, we present the follow-up efforts by our team for this particular event and the development of the pipeline. In Section 2, we discuss the S190426c event and how the source properties were revised over time. Observation strategy of GIT is presented in Section 3. Section 4 highlights our data reduction pipeline, including the newly developed image subtraction and candidate vetting pipeline. In Section 5, we show the candidates discovered – none of which are consistent with a kilonova. We discuss the implications of these non-detections in the context of various theoretical models. We conclude with a discussion and future outlook in Section 6.

## 2 S190426C

### 2.1 Discovery and initial updates

On 2019-04-26 at 15:47:06 UTC, the LIGO Virgo Collaboration issued a VOevent alert (Seaman et al. 2006) about a binary merger candidate S190426c.<sup>1</sup> There was a 49 per cent chance that this was a merger of two neutron stars (Table 1). However, the event had a low statistical significance, with one event per 1.6 yr FAR. The source was estimated to be at a distance of  $375 \pm 108$  Mpc with a 90 per cent credible sky area of  $1262 \text{ deg}^2$  (Ligo Scientific Collaboration & VIRGO Collaboration 2019a). The localization was divided into three major chunks: a ‘cap’ near the north pole, a long ‘banana’ in the Northern hemisphere, and a set of scattered ‘islands’ in the equatorial and southern regions (Fig. 1a). Based on internal discussions within

the GROWTH collaboration, it was decided that the GIT would observe the north polar cap ( $\delta \gtrsim 80^\circ$ ), with the Zwicky Transient Facility covering the northern banana and DECAM covering the south (Goldstein et al. 2019a,b).

The next day, a revised LALInference (Veitch et al. 2015) sky map was provided, which shrunk the 90 per cent region slightly to  $1131 \text{ deg}^2$ , while the luminosity distance estimate remained  $377 \pm 100$  Mpc (Ligo Scientific Collaboration & VIRGO Collaboration 2019b). This update removed most of the equatorial and southern localization regions (Fig. 1b).

### 2.2 Nature of the source

Ten days after the event, the event class probabilities were revised (Ligo Scientific Collaboration & VIRGO Collaboration 2019c), with a 60 per cent probability that the source was a Neutron Star–black hole merger (NSBH) and a 15 per cent chance that it was a binary neutron star (BNS) event. There was a 25 per cent chance that this was a ‘MassGap’ event, with the class defined such that one of the objects was in the  $3\text{--}5 M_\odot$  range. Three months after the event, LIGO Scientific Collaboration & Virgo Collaboration (2019) reported that the event was most likely terrestrial noise with the help of further analysis (Table 1). However, the probability of being astrophysical was non-zero.

Final offline analysis of the data (Abbott et al. 2020) shows that the masses of the two components were  $m_1 = 5.7_{-2.3}^{+4.0}$  and  $m_2 = 1.5_{-0.5}^{+0.8}$ ; a wide span encompassing black holes, neutron stars, and mass gap objects. This is also reflected in the final source class probabilities, which were not explicitly revised in the re-analysis. In our discussion (Section 6), we consider two possibilities for the nature of the source: a BNS merger and an NSBH merger.

## 3 OBSERVATIONS

### 3.1 The GIT

The GIT is a robotic optical telescope located at the Indian Astrophysical Observatory (IAO) (Cowsik, Srinivasan & Prabhu 2002; Stalin et al. 2008) in Hanle, Ladakh.<sup>2</sup> It is a 0.7-m planewave CDK700 telescope coupled with a 16-megapixel Andor iKon-XL camera. The telescope design and the wide-format camera together give the telescope a wide field of view (FoV). The high sensitivity non-vignetted area is best approximated as a  $0.67^\circ$  diameter circle. The pixel scale is 0.676

arcsec. Our typical limiting magnitude in the  $r'$  band is 20.5 ( $5\sigma$ ) in 5-min exposures and 21.0 in 10-min exposures. Since the commissioning of the telescope in 2018 June, we have steadily upgraded our software to make it fully autonomous. In early 2019, the telescope was being operated in a semi-autonomous ‘supervised observing’ mode, where remote observers were responsible merely for initiating various batch scripts and intervening only when there were errors. More details on GIT are available at Kumar et al. (2022).

### 3.2 Observing schedule

When S190426c was first reported, GIT was involved in the follow-up of the previous candidate S190425z (Bhalerao et al. 2019a; Waratkar et al. 2019a; Abbott et al. 2020). Based on the localization

<sup>1</sup><https://gracedb.ligo.org/api/superevents/S190426c/files/S190426c-1-Preliminary.xml,0>

<sup>2</sup><https://sites.google.com/view/growthindia/>

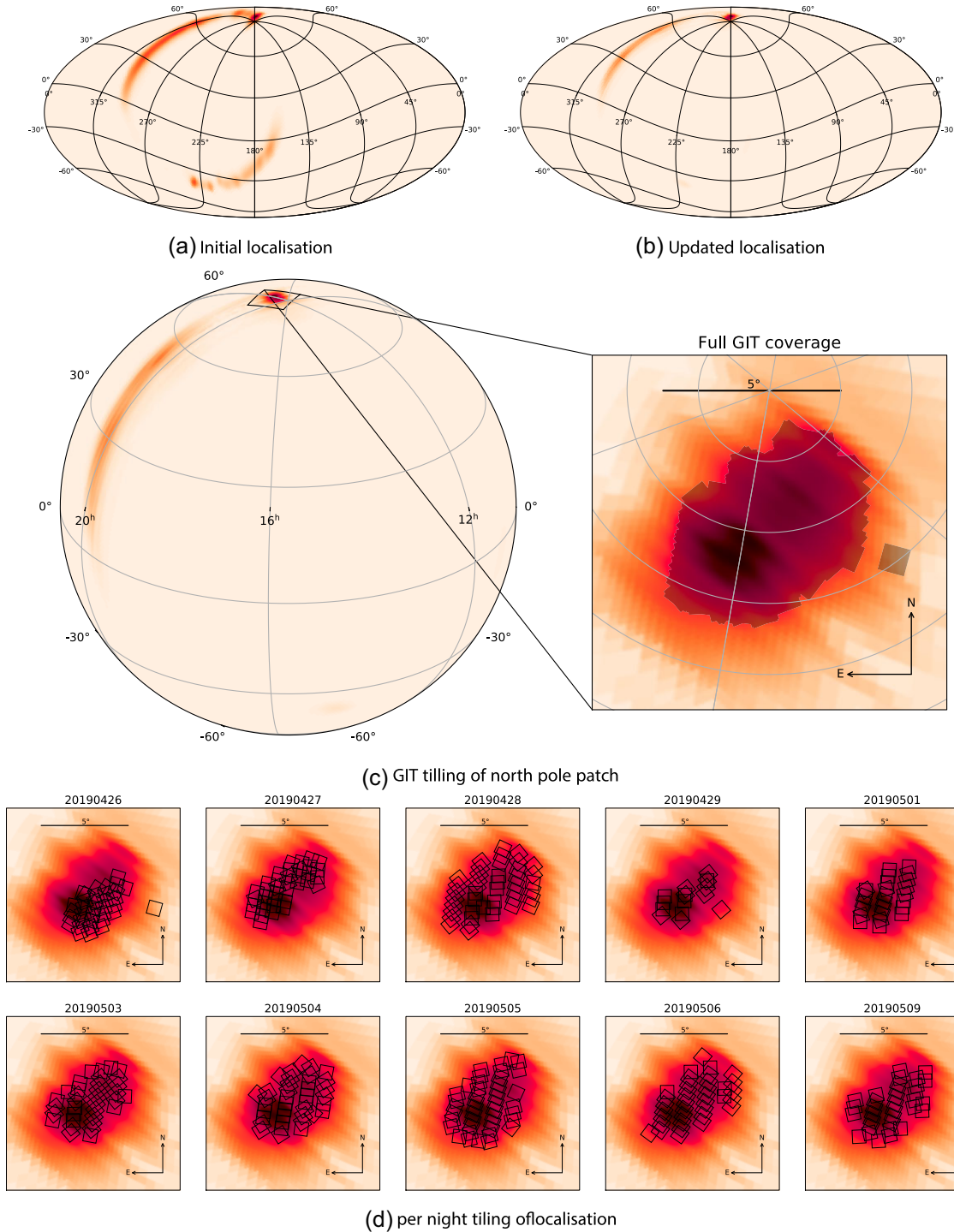


**Figure 1.** (a) First localization map circulated by LVC shows that a major portion of localization probability was in the Northern hemisphere with a couple of low probability patches in the Southern hemisphere. (b) Updated localization map by LVC along with GIT tiling indicated by grey shaded region. In updated localization, the probability gets shifted into the Northern hemisphere. (c) S190426c LALInference localization skymap with GIT tiling shown by squares. (d) Tiles were observed by GIT on each night of observation.

of the new event, we decided within the GROWTH collaboration that GIT would cover the northern polar cap (Bhalerao et al. 2019b), ZTF would cover the northern ‘banana’ (Perley et al. 2019; Coughlin et al. 2019d) and DECAM would cover the southern ‘islands’ (Andreoni et al. 2019; Goldstein et al. 2019a; Goldstein et al. 2019b). Accordingly, we created an observing schedule for GIT

from the GROWTH ToO Marshal (Coughlin et al. 2019a,c) using the ‘bayestar.fits’ skymap (Singer & Price 2016) and obtained 31  $r'$  images covering  $7.5 \text{ deg}^2$ , with 3.9 per cent probability of containing the GW source as per this original localization. Using the updated localization, this probability increased to  $\sim 6$  per cent (Coughlin et al. 2019d).

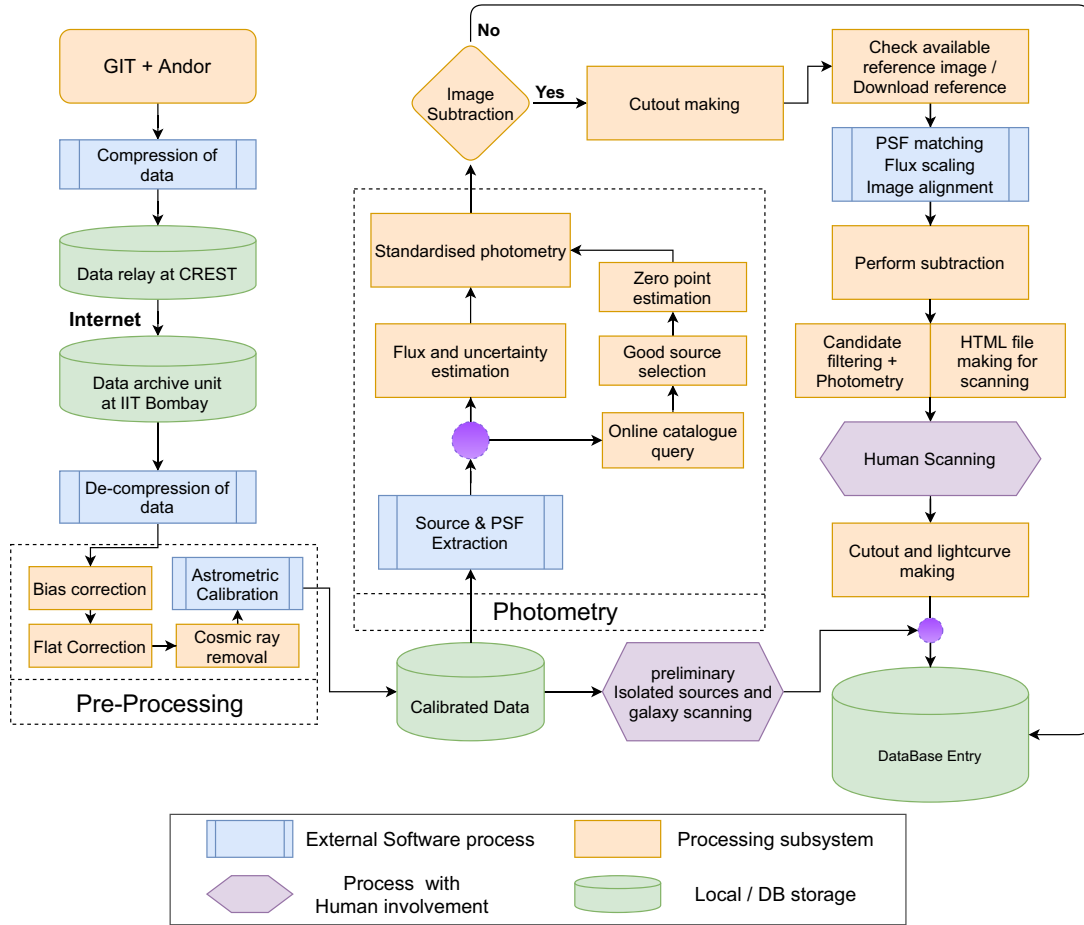


**Figure 2.** Data reduction pipeline flow of GIT. The light green elements indicate the local or data base storage system for data. Light blue boxes are external software dependencies. Light brown coloured boxes represent python bases processing subsystems. All processes are described in full detail in Section 4.

On subsequent nights, the revised localization meant that a larger probability region was accessible to GIT for imaging. With the  $0.5 \text{ deg}^2$  field of view of GIT, we carefully planned our observing sequences to maximize science returns. Theoretical models indicate that the optical counterparts to BNS/NSBH mergers will typically evolve on time-scales of a couple of days, or longer (Metzger et al. 2010; Roberts, Woosley & Hoffman 2010; Barnes & Kasen 2013; Tanaka et al. 2013; Kasen, Fernández & Metzger 2015). Hence, we divided the north polar cap into two partially overlapping offset grids that would be observed on alternate nights, covering about  $10 \text{ deg}^2$  each (Kumar et al. 2019; Waratkar et al. 2019b). Observations were scheduled using an implementation of the ‘Enhanced Array’ scheduling algorithm of Rana et al. (2017). Over the next two weeks, data were obtained for as many fields of these grids as possible (Fig. 1d). Each point in the showed region was typically observed 4-5 times in our ten observation epochs. Due to the partial overlap in fields within a grid and overlap between the two grids, some parts of the polar cap were observed as many as 10 times during our follow-up. Observations were missed on a few nights: 2019 April 30; May 2, 7, and 8 due to inclement weather.

The primary goal of GIT observations was to identify promising transient candidates, which could then be followed up by the 2-m Himalayan Chandra Telescope (for instance Pavana et al. 2019) or other GROWTH partners. Hence, we acquired images in a single filter ( $r'$ ) instead of multifilter combination usually preferred in follow-up of such events (Andreoni et al. 2022). Given the large median distance

of 375 Mpc in the initial LVC alert, we opted to take 600 s exposures, giving us a nightly median limiting magnitude of 20.5–21.5 (Fig. 4) depending on observing conditions. We continued observations for about two weeks to ensure that we would have light curves for any transient candidates and that any event with a late peak would not be lost.

## 4 DATA PROCESSING

Once the Target-of-Opportunity schedule is uploaded to the GIT control computer, it executes the observations and stores data locally at Hanle. The images are compressed using the lossless Rice compression algorithm using the `fpack` package (Pence, Seaman & White 2011). They are then automatically downloaded in real-time via satellite link to the CREST campus of the Indian Institute of Astrophysics (IIA), from where another script downloads them to the final processing system at the Indian Institute of Technology Bombay (IITB), where they are uncompressed for further processing.

### 4.1 Data reduction

The GIT data is reduced using the GROWTH-India Image Reduction Pipeline (GRIIPP). The pipeline is divided into three major parts: pre-processing, Point Spread Function (PSF) photometry, and image subtraction. Pre-processing includes generic steps like bias subtraction, flat-field correction, and cosmic ray removal using

**Table 2.** Filtering process of the good candidates from spurious candidates using vetting cuts. Candidates rejected in each step of vetting cut are listed in the third column. Column four represents the candidates survived after each cut.

Name	Description	Candidates rejected	Candidates left
Initial candidate	All sources identified as local maxima in $S_{\text{corr}}$ images.	–	2096 938
Faintness cut	Transients that are more than one magnitude fainter than the limiting magnitude of the image are rejected. This cut is designed to be conservative.	816 816	1280 122
Photometric uncertainty	Candidates with photometric uncertainties $> 1$ mag are rejected.	125 866	1154 256
Vignetting and edge cuts	We created a binary mask, and rejected sources suffer vignetting (outside a 46 arcmin circle) or are too close to cutout edges (5 pixels). Note that cutouts overlap by 100 pixels, so the latter step does not reject any source.	295 744	858 512
FWHM cut	We fit a one-dimensional (1D) Gaussian along the central row and then the central column of each candidate, to measure the FWHM ( $F_c$ ), and compared it with the FWHM of the full image PSF ( $F_p$ ). Only candidates with $0.5 < F_c/F_p < 1.5$ were accepted.	531 309	327 203
XY centre cuts	If the centres of the two Gaussian fits were discrepant by more than 10 pixels from each other, the candidates were rejected.	73 358	253 845
Duplicates and single detections	Since image subtraction was performed on overlapping cutouts, several sources were detected in multiple cutouts from the same parent image. These were merged. Any sources that were detected in only one parent image were rejected.	246 528	7 317
Bright candidate rejection	Given the luminosity distance of S190426c is $\geq 300$ Mpc, it is highly unlikely to have a kilonova candidate to be 16 magnitudes in brightness even with very high ejecta masses (Kasen, Fernández & Metzger 2015; Barbieri et al. 2019; Anand et al. 2021; Zhu et al. 2020)	441	6 876
Bright star proximity	Sources within 5 arcsec of any stars brighter than 15th magnitude in PS1 were rejected.	2 708	4 168
Visual inspection	Independent visual inspection by three people.	4 051	117
Grouping	multiple detections of same object grouped.	–	23
Star/galaxy separation	PS1 star-galaxy check.	18	5

**Table 3.** Detection efficiency of GIT image subtraction and candidate vetting pipeline. Raw efficiency indicates the number of sources retrieved using a pipeline with respect to injected sources. Coverage indicates the percentage of image portion coverage available in PS1 for a GIT cutout in a single query using `panstamps`. Note that coverage efficiency increased to  $\sim 93.5$  per cent in actual analysis after the tests had been completed. Effective efficiency is defined as the efficiency of GIT pipeline considering 100 per cent reference image coverage.

	Efficiency		Effective
	Raw	Coverage	
Filter efficacy test	78.8 per cent	84.6 per cent	93.1 per cent
Blind test	82.1 per cent	86.7 per cent	94.7 per cent

standard data reduction techniques. As a last step of pre-processing, astrometry is performed on images using the `solve-field` astrometry engine (Lang et al. 2010). The corners of the camera extend outside the usable field of the telescope, and we see strong vignetting effects. We limit our analysis to a  $\sim 42$  arcmin square box to exclude regions strongly affected by vignetting. After the pre-processing, images are used for performing PSF photometry as described in Kumar et al. (2022). The data reduction steps are depicted in Fig. 2. During reduction of the data obtained for event under discussion in this article, we developed an image subtraction and candidate vetting pipeline, which has been described in Section 4.3.

## 4.2 Quick-look searches

GIT had its first light in the summer of 2018, focusing on automation and reliably acquiring data. As a result, our image subtraction and transient pipelines were not ready when we undertook these follow-up observations. Our real-time processing was limited to two types of ‘quick-look’ searches:

*Search for isolated sources:* We used `SExtractor` to find all sources in our images and cross-matched these source lists with publicly available catalogues like PanSTARRS (Chambers et al. 2016) and SDSS (Aguado et al. 2019) to identify new objects in the images. Only a few significant candidates were found, but they all matched known minor planets in `mpchecker`<sup>3</sup> and were rejected for being unrelated to S190426c.

*Search for sources on galaxies:* In case the transient was located on a bright host, it is possible that `SExtractor` would not flag it as an independent point source. To cover such cases, we obtained a list of galaxies from the GLADE catalogue (Dályá et al. 2018) and from the NASA/IPAC Extragalactic Data base gravitational wave follow-up service.<sup>4</sup> For instance, 338 GLADE and 8 NED galaxies were present in fields imaged on the first night. We downloaded PanSTARRS thumbnails for each of these galaxies using the `panstamps` utility,<sup>5</sup> then blinked images in SAOImage DS9 (Joye & Mandel 2003) to look for changes. No transients were found in this search.

<sup>3</sup><https://minorplanetcenter.net/cgi-bin/checkmp.cgi>

<sup>4</sup>The service is currently hosted at [https://ned.ipac.caltech.edu/uri/NED::GW\\_Foverview/](https://ned.ipac.caltech.edu/uri/NED::GW_Foverview/).

<sup>5</sup><https://github.com/thespacedoctor/panstamps>

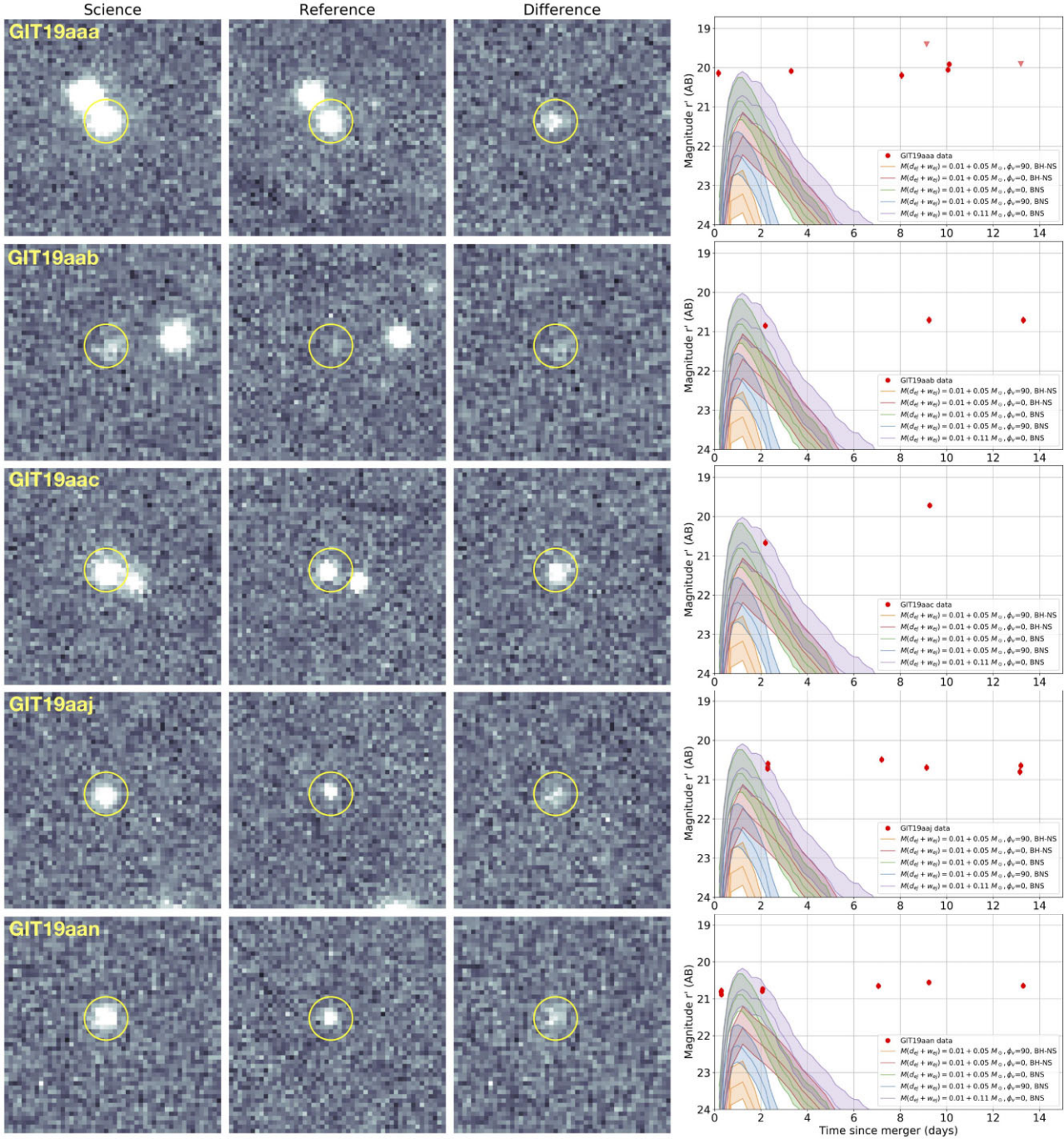


**Figure 3.** Five good candidates resulted from the GIT data after scanning. The first column represents cutout of candidates from GIT images, second and third columns show reference from PS1 and different images, respectively. The final columns shows  $r'$ -band light-curve comparison with the KN model (Heinzl et al. 2020) for each candidate. None of the candidates shows a promising light curve to qualify as kilonova (see Section 5).

### 4.3 Image subtraction pipeline

We undertake a more rigorous search for transients using the GIT image subtraction pipeline based on the ZOGY algorithm (Zackay, Ofek & Gal-Yam 2016). The pipeline is built using a combination of Astropy modules (Astropy Collaboration et al. 2013, 2018), *SEXtractor*, *PSFEx* (Bertin 2011), *SWarp* (Bertin 2010), *SCAMP* (Bertin 2006), and ZOGY-based pipeline (Guevel & Hosseinzadeh 2017) to perform subtraction.

The  $\sim 0.5$  deg<sup>2</sup> FoV of GIT makes it infeasible for us to have reference images from our telescope for the entire sky. Instead, we rely on PanSTARRS images (Flewelling 2018; Chambers et al. 2019), downloaded using *panstamps*, as reference images for our processing.

There are several factors that we need to handle before undertaking image subtraction. PS1 images are limited to a size of about 26 arcmin, and a *panstamps* query returns a cutout that contains the queried coordinate but is not necessarily centred on it. GIT images have an un-vignetted field of 46 arcmin and have a different position

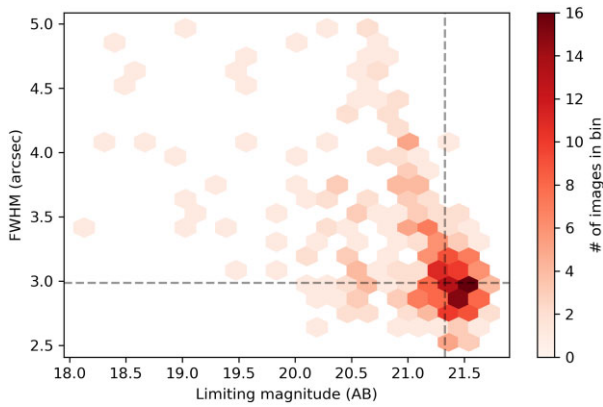


**Figure 4.** Statistics of ten nights’ data for S190426c. GIT reached a typical depth of 21.32 mag (vertical dotted line) with a median FWHM of 2.98 arcsec during observation (horizontal dotted line).

angle from the PanSTARRS cutouts. Furthermore, ZOGY-based image subtraction is a memory-intensive process, and processing the full 16-megapixel GIT image is infeasible on typical desktop computers. Lastly, there may be non-uniformities in response across the GIT image due to the relatively large image size and FoV. Zackay et al. (2016) recommend using relatively smaller images to minimize the effects of in-homogeneous transparency and residual astrometric shifts.

As a result, we divide the image into a  $4 \times 4$  grid of cutouts for image subtraction. The cutouts have an overlap of 100 pixels ( $\sim 1$  arcmin) to ensure that each source is completely present in at least one cutout. In targeted observing mode, if we are interested in just a particular target in the image, we create a single cutout centred on that target. We then seek a PanSTARRS image for the centre of each cutout. Since we were observing the same part of the sky repeatedly, first, a local query is done to see if the requested images already exist. If not, `panstamps` are used to download the image from the image server.

The next step is to match the GIT cutout to the reference image. We use `SExtractor` to extract sources from both science and reference images, using a detection threshold of  $5\sigma$ . Then we query the Gaia data release 2 (Gaia DR2) (Gaia Collaboration et al. 2018) catalogue for the area covered in the cutout. Using our `SExtractor` catalogues and the Gaia DR2 positions of sources, `SCAMP` calculates an astrometric solution and corrects astrometric errors between stars of the two input catalogues and the Gaia catalogue.

Next, we use `SWarp` to subtract the background from the cutout and reference image using a 64-pixel mesh and a filter of three mesh blocks. The images are then resampled to a common plate scale and pixel grid. In this process, fluxes are also re-scaled based on the local ratio of pixel scales, and weight maps are generated. Based on all these, `SWarp` also calculates the variances for images. These are added in quadrature to the Poisson noise estimates from the image to obtain Root-Mean Square images (RMS images) needed as an input for the ZOGY algorithm.

Hence, resampling changes the PSF of the images, so it needs to be estimated again. We run `SExtractor` on these resampled images to create catalogues of bright ( $\geq 10\sigma$ ) sources, which are used by `PSFEX` to create a PSF model. Bright, unsaturated and isolated sources in the cutout and reference images are used to calculate flux scaling, and astrometric uncertainties.

In the final step, the pipeline uses the cutout and reference images, the PSF model, RMS images, and astrometric uncertainties

to perform image subtraction and calculate the difference image. Another image called the score-corrected statistics image ( $S_{\text{corr}}$  image) is generated: local maxima in this image are given the location and statistical significance of the source detected in the difference image.

The data reduction pipeline is designed so that it can perform actions like stacking of images, subtractions over the full image, and subtraction on the specific targets individually. The pipeline is entirely automatic and takes approximately 2.5 min to fully reduce the GIT cutout (with image subtraction) on the current processing unit, which is an Intel(R) Core(TM) i7-6700 CPU running at 3.40 GHz supported by 16 GB of random access memory. The average time is calculated assuming that the PanSTARRS reference images are available in the local data base. The pipeline takes an extra 20 s to download the reference image using `panstamps` if necessary.

#### 4.4 Detecting transients in the difference image

We searched for candidates in the subtracted images and detected the local maxima in the  $S_{\text{corr}}$  image to detect the transients. Among all local peaks corresponding to transients, we choose transients with corrected score ( $S_{\text{corr}} > 5$ ). Using these criteria, we found a total of 2,096,938 candidates in all images, with the majority of these found to be artefacts. Cores of very bright stars in the original field show some residuals as they have extra Poisson noise sitting at their centre, giving rise to many spurious sources in the difference images. Also, the GIT images suffer from vignetting around the edges, contributing to many spurious sources. To eliminate these spurious sources, we developed a filtering process that applies various automated cuts to candidates. The steps used to reject spurious candidates are summarized in Table 2.

After automatic cuts, we were left with 4168 detections scanned manually by three observers independently. A majority of the sources were discarded during manual scanning as those were a result of either bad subtraction or residuals of cosmic rays which did not get removed cleanly. The number of good candidates went down to 23 with 117 detections after the manual scanning. Note that all candidates here had multiple detections – we would have rejected any objects with just one detection. All candidates had underlying sources associated with them. Therefore, we checked these underlying sources for stellar or non-stellar (galaxy) classification with the help of the PS1 catalogue using the method described in Farrow et al. (2014). All but five sources were found to be stellar. We performed a standard check on MPC for these five remaining candidates to ensure that none of them is a moving object.

#### 4.5 Coverage efficiency

Some complexity is added to our pipeline due to two factors: 1) the position angle of GIT images is not the same as the reference images, and 2) `panstamps` returns a reference image that contains the queried point (centre of our image), but not necessarily at the centre of the PS1 cutout. As a result, we regularly see ‘holes’ where image subtraction could not be performed as the area was outside the reference image. This problem seems to be exacerbated by the fact that our observations are close to the pole. At the first pass, the holes occupied  $\sim 15$  per cent of our observed fields, giving us a net ‘coverage efficiency’ of  $\sim 85$  per cent. Currently, we have a script that helps us identify such holes, and we re-run the pipeline by downloading reference images for those hole centres, which increases the coverage to  $\sim 93.5$  per cent

## 4.6 Detection efficiency

As discussed in Section 4.4, the large number of initial candidates were reduced by various filtering steps, followed by human inspection. Presently, we lack a machine learning-based real-bogus candidate classifier. In order to check the reliability of our procedure, we undertook various tests.

First, we tested the efficacy of the filtering process before human inspection. We created fake sources using the PSF of the images and injected them at random locations in the images. A total of 3100 sources spanning over magnitude range  $\in[18.5-20.5]$  were injected across various fields in  $g'$  and  $r'$  filter images. 476 of these were lost to coverage issues, leaving 2624 ‘retrievable’ candidates. In the actual pipeline, the first candidate identification step post-image subtraction included 2490 sources flagged as candidates in the first step. In addition to the injected sources, about 124 000 spurious sources were flagged as candidates at this stage. After applying the filter criteria, the number of spurious sources drastically decreased to  $\sim 4550$ , while only 48 injected sources were lost. Thus, in the end, human scanners would have inspected  $\sim 7000$  candidates, and recovered  $\sim 93$  per cent of the injected sources.

Next, we performed a complete end-to-end test ‘blind test’ including human scanning, using raw data from our S190426c observations. In each image, we injected between 0–7 sources. Each injected source was repeated in multiple images to test our ability to find multiple detections. The number of repetitions was randomly selected between 4 and 7. The human scanners were unaware of the source locations, magnitudes, and number of repetitions. We obtained comparable results, with an effective efficiency of  $\sim 95$  per cent (Table 3). Note that the tests were not repeated after we introduced a script that filled coverage holes (Section 4.5), which will boost the raw efficiency and hence the raw efficiency by 8–9 per cent.

We also explored the possibility of using `SExtractor` to directly find sources in the difference images. We selected only those candidates which did not raise any `SExtractor` FLAGS<sup>6</sup> (FLAGS = 0) and with the source FWHM in the range of 0.5–1.5 times the nominal PSF. We found that the detection efficiency for this method is only about 70 per cent, significantly lower than the ZOGY  $S_{\text{corr}}$  method.

## 5 RESULTS

### 5.1 Candidates

Our search process yielded five candidates that passed our filters and had more than one detection each, which we now discuss in detail. First detection images for these 5 candidates along with their full light curves during our observations are shown in Fig. 3. The figure also shows representative kilonovae light curves, which we discuss in Section 5.2

*GIT19aaa*: This candidate was first detected  $\sim 0.17$  d after the event trigger. The candidate was detected four more times on subsequent night observations, with upper limits in two observations. The candidate shows little or no evolution over the two weeks of observations.

*GIT19aab*: The field of this candidate was first observed  $\sim 2.18$  d after the event, where we obtained our first detection. The candidate was also detected in subsequent imaging epochs 9.24 and 13.3 d after the trigger, with no non-detections in our full observing period. *GIT19aab* has nearly a constant magnitude over this timespan.

*GIT19aac*: Similar to *GIT19aab*, this candidate was also observed and detected  $\sim 2.17$  d after the trigger. This candidate brightens by nearly a magnitude over 7 d, which is not expected from kilonovae.

*GIT19aaaj*: This candidate was first detected  $\sim 2.28$  d after the trigger. It is located in the overlapping area of certain GIT tiles, resulting in multiple observations on some epochs. It has a relatively flat light curve, with signs of intra-night variability. There is an underlying source present at the location of the source, which has a history of variability as per the PS1 Catalogue. Therefore, we conclude that the candidate is likely a result of activity in the underlying source and is not associated with S190426c.

*GIT19aan*: This candidate was detected on the first night of observation itself  $\sim 0.27$  d after the GW event. An almost flat light curve with seven detections over a period of 13 d indicates that this candidate is not associated with the S190426c.

In summary, four candidates did not show any significant temporal evolution, while one brightened very slowly. These behaviours are inconsistent with expectations from kilonovae, and we can rule out all of our candidates as potential counterparts to S190426c.

### 5.2 Implications of non-detection

The initial classification of S190426c indicated that it may be BNS or an NSBH event. Hence, we consider representative theoretical models for both merger types and calculate the expected light curves from both. We compare these to our candidates (Fig. 3) and also to our non-detection upper limits (Fig. 5), to constrain the merger ejecta mass. Inspired by Bulla (2019), Dietrich et al. (2020), we picked a plausible scenario with an ejecta opening angle of  $30^\circ$  for models discussed in this section.

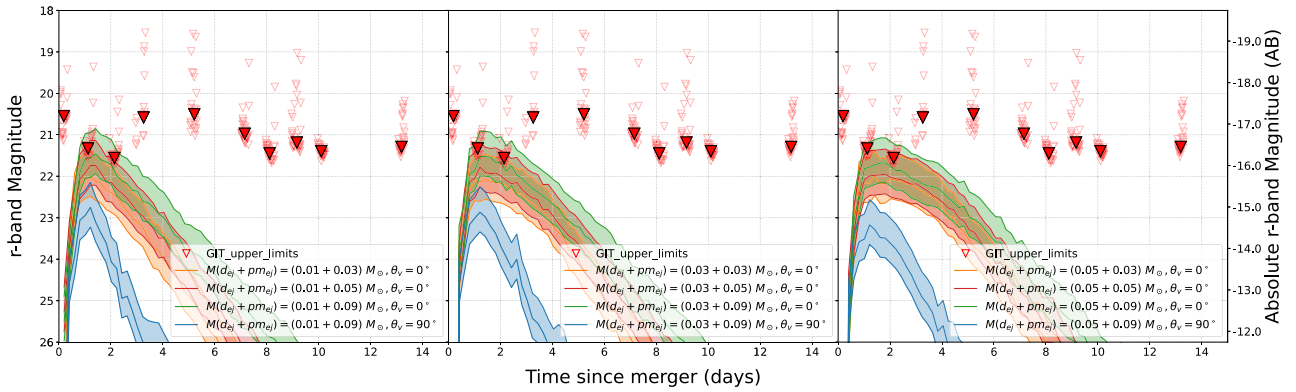
#### 5.2.1 Neutron Star–Black Hole merger models

We compared our  $r'$  band upper limits to light curves simulated with `POSSIS` (Bulla 2019; Anand et al. 2021) for NSBH models. `POSSIS` is a radiative transfer simulation code that provides simulated light curves for the KNe model. This code generates light curves for NSBH as well as BNS model considering ejecta mass from dynamical and post-merger components of ejecta. A wide range of viewing angles from polar view ( $\theta_v = 0^\circ$ ) to equatorial view ( $\theta_v = 90^\circ$ ) are considered by the code while generating the light curves. We used various possible combinations of ejecta mass from dynamical and post-merger components:  $M(d_{\text{ej}}) = [0.01, 0.03, 0.05] M_\odot$  and  $M(\text{pm}_{\text{ej}}) = [0.03, 0.05, 0.09] M_\odot$  to compare our observations with simulated light curves.

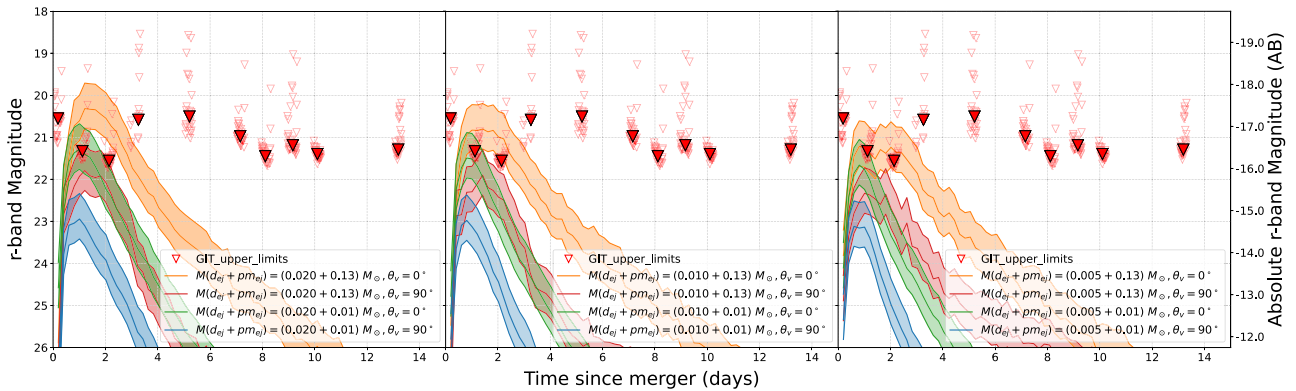
Fig. 5(a) depicts the simulated  $r'$  light curve for the NSBH models with various combinations of dynamical and post-merger ejecta masses. The rest-frame luminosity is converted into an apparent magnitude based on the distance to this source. The shaded band for each model denotes the  $1\sigma$  range of distances, while the solid central line is calculated using the median distance of 353.2 Mpc for the region covered by GIT. The corresponding absolute magnitudes are shown on the right side axis. The red triangles denote the depth of GIT images. Since no counterpart was found, these indicate the upper limits to the brightness of a putative counterpart located in this part of the sky. Thus, if this is an NSBH event for which the true counterpart was in the region observed by GIT, we find that a scenario with  $M(\text{pm}_{\text{ej}}) > 0.09 M_\odot$  is very unlikely for polar viewing angles. For edge-on/equatorial view ( $\theta_v = 90^\circ$ ), the counterparts are expected to be fainter and evolve faster, and would be beyond the detection capabilities of GIT.

<sup>6</sup><https://sextractor.readthedocs.io/en/latest/Flagging.html>





(a) NSBH model for different ejecta mass and viewing angle (absolute).



(b) BNS model for a few ejecta mass and viewing angle possibilities (absolute).

**Figure 5.** Constraining KN models based on GIT upper limits. The coloured bands indicate the expected range of magnitudes over the  $1\sigma$  distance range of the source. The left axis indicates the apparent magnitude, while the right axis shows the source absolute magnitude at the median localization distance. Different coloured bands show different source models. *Upper panels:* NSBH merger models. *Lower panels:* BNS merger models.

We also considered the NSBH KNe model by Kawaguchi, Shibata & Tanaka (2020) that explores the scenario of prompt collapse to form a black hole in compact object mergers using radiative transfer simulations (Fig. 6, upper panel). We select two combinations of dynamical and post-merger ejecta masses ( $M(d_{ej} + pm_{ej}) \leq 0.02 + 0.02 M_{\odot}$  and  $M(d_{ej} + pm_{ej}) \leq 0.04 + 0.01 M_{\odot}$ ), seen at head-on and face-on inclinations seen from a range  $\in [0^{\circ}, 90^{\circ}]$  of viewing angle are compared to our observations. These models predict a faster evolution of the counterpart, highlighting the importance of early observations. Note that the model is not very reliable during the first-day post-merger (grey shaded region in Fig. 6). Thus, the most important data is our upper limit at 2 d after the event, which disfavours an event with a polar viewing angle and high dynamical ejecta, located up to a distance of  $\sim 300$  Mpc.

### 5.2.2 Binary Neutron Star models

We now consider a series of BNS counterpart models and compare them to our upper limits. Fig. 5(b) shows the plotted simulated light curves for  $M(d_{ej}) = [0.02, 0.01, 0.005] M_{\odot}$  for a very low and very high post-merger ejecta masses ( $0.01 M_{\odot}$  and  $0.13 M_{\odot}$ , respectively), for polar and equatorial viewing angles. GIT data can rule out the high post-merger ejecta mass cases for polar viewing angles (assuming the counterpart was located in the observed part of the sky). The low ejecta mass cases are ruled out if the source was

located in the lower side of the allowed distances ( $d \lesssim 300$  Mpc). We cannot strongly constrain the cases with low masses of post-merger ejecta.

Next, we consider the Banerjee et al. (2020) blue KN model for BNS merger counterparts, which provides precise opacity calculations at early times. We see that our observations one day after the merger can completely rule out the scenario with dynamical and post-merger ejecta masses of  $0.02 M_{\odot}$  and  $0.05 M_{\odot}$ .

Lastly, we consider the KNe model by Hotokezaka & Nakar (2020),<sup>7</sup> very high ejecta mass model  $M_{ej} = 0.3 M_{\odot}$  can be completely ruled out as shown in the lower right-hand panel of Fig. 6. The  $0.1 M_{\odot}$  case can be constrained to require  $d \gtrsim 300$  Mpc to be non-detectable by GIT. However, an event similar to GW170817 ( $M_{ej} = 0.005 M_{\odot}$ ) at these distances would be undetectable by GIT.

In conclusion, GIT observations at early times can effectively rule out bright counterpart models, but are not deep enough to constrain the fainter models.

## 6 SUMMARY AND FUTURE OUTLOOK

The GROWTH-India Telescope participated in a coordinated distributed campaign to search the localization region of S190426c

<sup>7</sup>These models are available at <https://github.com/hotokezaka/HeatingRate>

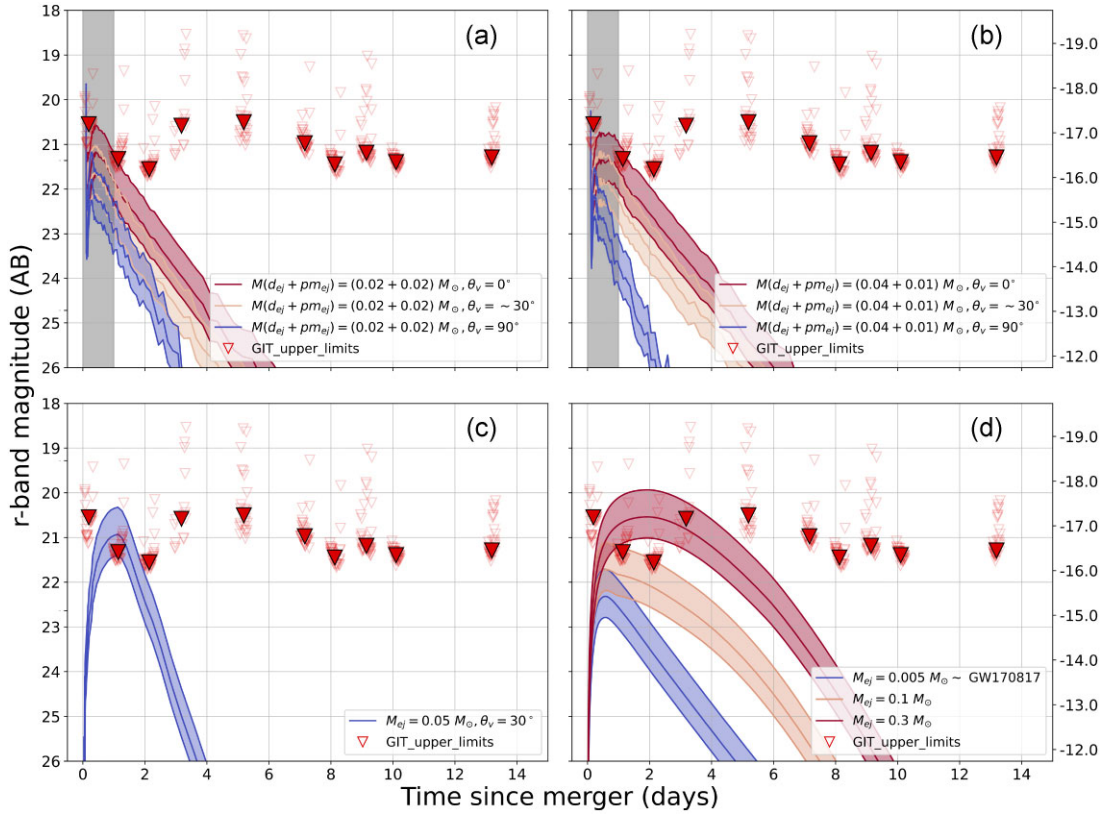


**Figure 6.** Constraining source emission models using GIT data. The bands and magnitudes are as described in Fig. 5. Panels a and b: Kawaguchi et al. (2020) NSBH models, with blue denoting an equatorial viewing angle and redder colours indicating a polar view. The models are not very reliable for the first day, which is shown as a shaded grey region. Panel c: Our data rules out the Banerjee et al. (2020) blue KN model. Panel d: We can rule out the high ejecta mass case for Hotokezaka & Nakar (2020) models (red curve), and constrain the distance to  $\gtrsim 300$  Mpc for moderate ejecta mass (orange curve).

for electromagnetic counterparts. GIT observed the northern polar cap, with the central and southern regions being observed by ZTF and DECam, respectively. We covered  $22.1 \text{ deg}^2$  region of the sky, which had a 17.5 per cent probability of containing the counterpart. We created an alternate-night observing programme and imaged the region for a total of 10 d, with each point imaged multiple times so that we could trace the evolution of any candidate counterpart. We attained a typical  $5\sigma$  limiting magnitude of 21.3 in our 10-min exposures, and point sources had a medium FWHM of 3 arcsec.

We imaged 8 NED and 332 glade galaxies, all of which were immediately visually searched for counterparts. We did not find any candidate counterparts in this search. We then developed a complete image subtraction and transient search pipeline, which was used to process the data and look for transients. Our tests show that we have a recovery rate of  $\sim 94$  per cent in such searches, though the actual ‘raw’ efficiency was lower due to incomplete reference image coverage.

We discovered 23 transients, of which five were flagged as potential candidates, while the rest were associated with stellar sources. The light curve evolution showed that none of the candidates was consistent with being a counterpart of S190426c. We thus obtained upper limits on the peak flux, and hence the peak luminosity of a possible counterpart for the probability region covered by our observations. We compared our upper limits to various theoretical models for counterparts to BNS and NSBH mergers. We find that we can rule out models with high ejecta mass in all cases. Our upper limits are sensitive enough to rule out a few more models in

the closer part ( $\lesssim 300$  Mpc) of the GW localization volume. Our data are most useful in the first few days after the trigger, where the emission is expected to peak. Beyond  $\sim 5$  d after the GW event, most models predict significantly fainter emission, which cannot be detected by GIT at large distances. Such continued follow-up with meter-class telescopes continues to be important for nearby events like GW170817.

An increase in sensitivity of advanced LIGO detectors resulted in a significant increase in the detection of triggers with a non-zero probability of a neutron star as one of the merger objects: from a single event in O2 to fifteen triggers during O3 (Abbott et al. 2020). The larger sky areas and increased distances in the localization volumes (Abbott et al. 2020) necessitate a large number of images, each with increased depth. This poses a formidable challenge for smaller telescopes like GIT to cover significant portions of the sky regions. Increased sensitivity of LIGO and Virgo detectors as well as the participation of KAGRA in the subsequent observing runs will improve localization for nearby events but will also add a large number of distant, poorly localized events (Petrov et al. 2022). Telescope networks, and small telescopes in particular, need better strategies to deal with this scenario.

Follow-up of BNS and NSBH triggers remains a high priority for GIT, and we will invest significant time to triggers in the fourth GW observing run (O4) and beyond. The follow-up strategy – tiling the localization region, galaxy targeted search, and photometric follow-up of external candidates – will be evaluated on a case-by-case basis for each trigger. Our data processing and photometric pipelines are

well-developed to enable rapid turn-around for targeted searches (Kumar et al. 2022). We are developing our image subtraction and transient search pipelines to increase our capabilities for blind searches for transients in our images. The improved pipelines will shorten the processing time, decrease the amount of human involvement needed, and more effectively discard spurious sources. Armed with these developments, we are confident that GIT will continue to play its role as a key resource for the electromagnetic follow-up of gravitational wave sources in the eastern hemisphere.

## ACKNOWLEDGEMENTS

The GROWTH India Telescope (GIT) is a 70-cm telescope with a 0.7-degree field of view, set up by the Indian Institute of Astrophysics and the Indian Institute of Technology Bombay with support from the Indo-US Science and Technology Forum (IUSSTF) and the Science and Engineering Research Board (SERB) of the Department of Science and Technology (DST), Government of India. It is located at the Indian Astronomical Observatory (Hanle), operated by the Indian Institute of Astrophysics (IIA). We acknowledge funding by the IITB alumni batch of 1994, which partially supports operations of the telescope. Telescope technical details are available at <https://sites.google.com/view/growthindia/>.

This research has made use of the NASA/IPAC Extragalactic Data base (NED), which is funded by the National Aeronautics and Space Administration and operated by the California Institute of Technology.

This research has made use of data and/or services provided by the International Astronomical Union's Minor Planet Center.

This research has made use of the VizieR catalogue access tool, CDS, Strasbourg, France (DOI : 10.26093/cds/vizie). The original description of the VizieR service was published in 2000, A&AS 143, 23.

This research has made use of NASA's Astrophysics Data System.

HK thanks the LSSTC Data Science Fellowship Programme, which is funded by LSSTC, NSF Cybertraining Grant #1829740, the Brinson Foundation, and the Moore Foundation; his participation in the programme has benefited this work.

MC acknowledges support from the National Science Foundation with grant numbers PHY-2010970 and OAC-2117997.

## DATA AVAILABILITY

All data used in this article have been included in a tabular format within the article.

## REFERENCES

Abbott B. P. et al., 2016, *Phys. Rev. Lett.*, 116, 061102  
 Abbott B. P. et al., 2017a, Centennial of General Relativity: A Celebration.  
 Abbott B. P. et al., 2017b, *Phys. Rev. Lett.*, 119, 161101  
 Abbott B. P. et al., 2017c, *ApJ*, 848, L12  
 Abbott B. P. et al., 2017d, *ApJ*, 848, L13  
 Abbott R. et al., 2020, *Phys. Rev. X*, 11, 021053  
 Aguado D. S. et al., 2019, *ApJS*, 240, 23  
 Anand S. et al., 2021, *Nat. Astron.*, 5, 917  
 Andreoni I. et al., 2019, GRB Coordinates Netw., 24268, 1  
 Andreoni I. et al., 2022, *ApJS*, 260, 18  
 Astropy Collaboration et al., 2013, *A&A*, 558, A33  
 Astropy Collaboration et al., 2018, *AJ*, 156, 123  
 Banerjee S., Tanaka M., Kawaguchi K., Kato D., Gaigalas G., 2020, *ApJ*, 901, 29

Barbieri C., Salafia O. S., Perego A., Colpi M., Ghirlanda G., 2019, *A&A*, 625, A152  
 Barnes J., Kasen D., 2013, *ApJ*, 775, 18  
 Bertin E., 2006, in Gabriel C., Arviset C., Ponz D., Enrique S., eds, ASP Conf. Ser. Vol. 351, Astronomical Data Analysis Software and Systems XV. p. 112  
 Bertin E., 2010, Astrophysics Source Code Library, record ascl:1010.068  
 Bertin E., 2011, in Evans I. N., Accomazzi A., Mink D. J., Rots A. H., eds, ASP Conf. Ser. Vol. 442, Astronomical Data Analysis Software and Systems XX. p. 435  
 Bhalerao V., Kumar H., Karambelkar V., Waratkar G., Sharma Y., Anupama G. C., 2019a, GRB Coordinates Netw., 24201, 1  
 Bhalerao V., Kumar H., Karambelkar V., Deshmukh K., Saraogi D., Anupama G. C., Stanzin T., Stanzin J., 2019b, GRB Coordinates Netw., 24258, 1  
 Bulla M., 2019, *MNRAS*, 489, 5037  
 Chambers K. C. et al., 2016, preprint (arXiv:1612.05560)  
 Chambers K. C. et al., 2019, The Pan-STARRS1 Surveys. preprint (arXiv:1612.05560)  
 Coughlin M. W. et al., 2019a, *PASP*, 131, 048001  
 Coughlin M. W., Dietrich T., Margalit B., Metzger B. D., 2019b, *MNRAS*, 489, L91  
 Coughlin M. W. et al., 2019c, *ApJ*, 885, L19  
 Coughlin M. W. et al., 2019d, GRB Coordinates Net., 24283, 1  
 Coughlin M. W. et al., 2020, *Nat. Commun.*, 11, 4129  
 Coulter D. A. et al., 2017, *Science*, 358, 1556  
 Cowsik R., Srinivasan R., Prabhu T. P., 2002, *Bull. Astron. Soc. India*, 30, 105  
 Cutler C., Thorne K. S., 2002, in Bishop N. T., Maharaj S. D., eds, Proc. 16th Int. Conf., General Relativity and Gravitation. p. 72  
 D'Avanzo P. et al., 2018, *A&A*, 613, L1  
 Dálya G. et al., 2018, *MNRAS*, 479, 2374  
 Dietrich T., Coughlin M. W., Pang P. T. H., Bulla M., Heinzel J., Issa L., Tews I., Antier S., 2020, *Science*, 370, 1450  
 Dietrich T., Coughlin M. W., Pang P. T. H., Bulla M., Heinzel J., Issa L., Tews I., Antier S., 2020, *Science*, 370, 1450  
 Drout M. R. et al., 2017, *Science*, 358, 1570  
 Evans P. A. et al., 2017, *Science*, 358, 1565  
 Farrow D. J. et al., 2014, *MNRAS*, 437, 748  
 Flewelling H., 2018, AAS Meeting Abstracts, #231  
 Gaia Collaboration et al., 2018, *A&A*, 616, A1  
 Ghirlanda G. et al., 2019, *Science*, 363, eaau8815  
 Goldstein A. et al., 2017, *ApJ*, 848, L14  
 Goldstein D. A. et al., 2019a, *ApJ*, 881, L7  
 Goldstein D. A. et al., 2019b, GRB Coordinates Netw., 24257, 1  
 Guevel D., Hosseinzadeh G., 2017, Dguevel/Pyzogy: Initial Release.  
 Hallinan G. et al., 2017, *Science*, 358, 1579  
 Heinzel J. et al., 2020, *MNRAS*, 502, 3057  
 Hotokezaka K., Nakar E., 2020, *ApJ*, 891, 152  
 Hotokezaka K., Nakar E., Gottlieb O., Nissanke S., Masuda K., Hallinan G., Mooley K. P., Deller A. T., 2019, *Nature Astronomy*, 3, 940  
 Joye W. A., Mandel E., 2003, in Payne H. E., Jędrzejewski R. I., Hook R. N., eds, ASP Conf. Ser. Vol. 295, Astronomical Data Analysis Software and Systems XII. p. 489  
 KAGRA Collaboration et al., 2021, accepted in Progress of Theoretical and Experimental Physics, preprint (arXiv:2008.02921)  
 Kasen D., Fernández R., Metzger B. D., 2015, *MNRAS*, 450, 1777  
 Kasen D., Fernández R., Metzger B. D., 2015, *MNRAS*, 450, 1777  
 Kasliwal M. M. et al., 2017, *Science*, 358, 1559  
 Kawaguchi K., Shibata M., Tanaka M., 2020, *ApJ*, 889, 171  
 Kumar H., Karambelkar V., Bhalerao V., Deshmukh K., Khandagale M., Anupama G. C., Stanzin T., Stanzin U., 2019, GRB Coordinates Netw., 24351, 1  
 Kumar H. et al., 2022, *AJ*, 164, 90  
 Lamb G. P., Kobayashi S., 2018, *MNRAS*, 478, 733  
 Lang D., Hogg D. W., Mierle K., Blanton M., Roweis S., 2010, *AJ*, 139, 1782  
 LIGO Scientific Collaboration, Virgo Collaboration, 2019, GRB Coordinates Netw., 25549, 1

- Ligo Scientific Collaboration, VIRGO Collaboration, 2019a, GRB Coordinates Netw., 24237, 1
- Ligo Scientific Collaboration, VIRGO Collaboration, 2019b, GRB Coordinates Netw., 24277, 1
- Ligo Scientific Collaboration, VIRGO Collaboration, 2019c, GRB Coordinates Netw., 24411, 1
- LIGO Scientific Collaboration et al., 2015, *Class. Quantum Gravity*, 32, 074001
- Lippuner J., Fernández R., Roberts L. F., Foucart F., Kasen D., Metzger B. D., Ott C. D., 2017, *MNRAS*, 472, 904
- Losurdo G., 2017, *Nuovo Cimento C Geophys. Space Phys. C*, 40, 120
- Margalit B., Metzger B. D., 2017, *ApJ*, 850, L19
- Metzger B. D. et al., 2010, *MNRAS*, 406, 2650
- Nakar E., Gottlieb O., Piran T., Kasliwal M. M., Hallinan G., 2018, *ApJ*, 867, 18
- Pavana M., Anupama G. C., Kiran B. S., Bhalerao V., 2019, GRB Coordinates Netw., 24200, 1
- Pence W., Seaman R., White R., 2011, Fpack and Funpack User's Guide: FITS Image Compression Utilities. preprint ([arXiv:1112.2671](https://arxiv.org/abs/1112.2671))
- Perley D. A. et al., 2019, GRB Coordinates Netw., 24331, 1
- Petrov P. et al., 2022, *ApJ*, 924, 54
- Pian E. et al., 2017, *Nature*, 551, 67
- Radice D., Perego A., Zappa F., Bernuzzi S., 2018, *ApJ*, 852, L29
- Rana J., Singhal A., Gadre B., Bhalerao V., Bose S., 2017, *ApJ*, 838, 108
- Rezzolla L., Most E. R., Weih L. R., 2018, *ApJ*, 852, L25
- Roberts L. F., Woosley S. E., Hoffman R. D., 2010, *ApJ*, 722, 954
- Seaman R. et al., 2006, Sky Event Reporting Metadata (VOEvent) Version 1.11. IVOA Recommendation 1 November 2006
- Singer L. P., Price L. R., 2016, *Phys. Rev. D*, 93, 024013
- Stalin C. S., Hegde M., Sahu D. K., Parihar P. S., Anupama G. C., Bhatt B. C., Prabhu T. P., 2008, *Bull. Astron. Soc. India*, 36, 111
- Tanaka M., Hotokezaka K., Kyutoku K., Wanajo S., Kiuchi K., Sekiguchi Y., Shibata M., 2013, *ApJ*, 780, 31
- The LIGO Scientific Collaboration et al., 2021, preprint ([arXiv:2108.01045](https://arxiv.org/abs/2108.01045))
- Valenti S. et al., 2017, *ApJ*, 848, L24
- Veitch J. et al., 2015, *Phys. Rev. D*, 91, 042003
- Waratkar G., Kumar H., Bhalerao V., Stanzin J., Anupama G. C., 2019a, GRB Coordinates Netw., 24304, 1
- Waratkar G., Kumar H., Bhalerao V., Karambelkar V., Anupama G. C., Stanzin J., 2019b, GRB Coordinates Netw., 24316, 1
- Zackay B., Ofek E. O., Gal-Yam A., 2016, *ApJ*, 830, 27
- Zhu J.-P., Yang Y.-P., Liu L.-D., Huang Y., Zhang B., Li Z., Yu Y.-W., Gao H., 2020, *ApJ*, 897, 20

This paper has been typeset from a  $\text{\TeX}/\text{\LaTeX}$  file prepared by the author.